Granular bed consolidation, creep and armoring under subcritical fluid flow

Benjamin Allen and Arshad Kudrolli
Department of Physics, Clark University, Worcester, MA 01610
(Dated: December 29, 2017)

We show that a freshly sedimented bed composed of spherical grains settles and creeps forward over extended periods under an applied hydrodynamic shear stress τ^*, which is below the critical value τ_c^* for bedload transport. The rearrangements are found to last at least over millions of times the sedimentation time scale of a grain in the fluid. Compaction occurs throughout the bed, but creep is observed to decay exponentially with depth, and decreases over time. The granular volume fraction in the bed is found to increase logarithmically, saturating at the random close packing value $\phi_{rcp} \approx 0.64$, while the surface roughness is on average essentially unchanged. Thus, we find that bed armoring occurs due to a deep shear-induced relaxation of the bed toward the volume fraction associated with the glass transition.

The response of a granular bed to a fluid flowing over its surface is important to the evolution of rivers and beaches, among many other geophysical and industrial systems. The onset of erosion and bed transport has been studied in the field and in large scale flumes for over a century [1], but with mixed results because of the difficulty in making measurements under such conditions [2, 3]. Therefore, a number of experiments and simulations have been performed more recently focusing on idealized monodisperse granular beds under model fluid flows [4–8]. A material dependent formula for the onset of a grain's motion has been developed [9]. The grain dynamics above the onset of bedload transport have been investigated with index matching techniques [5, 7, 8, 10, 11], and granular velocities have been shown to decay exponentially into the bed under steady state conditions [8]. Nonetheless, many important questions pertaining to the onset of erosion and the state of the bed remain.

While a steady granular flow at the bed surface is observed above a critical hydrodynamic shear stress τ_c^*, history-dependent transient flow has been noted below this value [4, 7, 8, 12, 13]. Because the applied shear stress τ^* is assumed to be unchanged, the bed becomes resistant to erosion up to a higher τ^* as the transients die out. Although this bed armoring has been observed in polydisperse beds, when smaller grains erode leaving behind larger grains which require a higher shear to erode, it was noted more recently that armoring can occur in essentially monodisperse beds accompanied by a decrease in bed height [4, 12, 13]. It remains unclear if the armoring arises due to surface rearrangements, whereby grains which protrude further into the fluid are selectively dislodged, or if the resistance to shear arises due to rearrangements deeper within the bed.

Further, in the case of dry frictionless granular materials, it has been noted that grains rearrange even under vanishingly small stress [14]. Long-term stress relaxation is known to occur post-slip across fault lines [15–18], and compaction of vibrated granular packings in gravity have been observed to evolve logarithmically [19–21]. However, the bed structure has not been studied in any significant detail to understand the corresponding dynamics under sub-critical hydrodynamic shear.

Here, we use internal imaging and results drawn from the study of granular compaction and jamming to understand the response of a bed composed of monodisperse spherical grains to fluid flow, below the threshold for bedload transport. Starting from a freshly sedimented bed, we investigate the spatial evolution of the bed at the grain scale away from the influence of side walls by using fluids with the same refractive index as the transparent grains. We then measure the spatio-temporal evolution of the bed as a function of imposed τ^* to understand the correlation of compaction, creep and the surface roughness over long times.

Fig. 1(a) shows the schematic of the circular flume apparatus consisting of a cylindrical container with radius $R_c = 90\,\mathrm{mm}$ with a conical top plate which can be rotated with prescribed frequency f to apply uniform shear to the fluid within [8]. Acrylic spheres with diameter $d = 1.52 \pm 0.01\,\mathrm{mm}$, density $\rho_g = 1180\,\mathrm{kg\,m^{-3}}$, and index of refraction $n = 1.4923 \pm 0.0003$ are filled to a height of approximately $10d$. The bottom of the container has a roughness $k = 0.5\,\mathrm{mm}$ to prevent hexagonal crystallization from occurring to model typical random packings in deep granular beds. The fluid has density $\rho_f = 1002\,\mathrm{kg\,m^{-3}}$ and kinematic viscosity $\nu = 0.018\,\mathrm{Pa\,s}$, and its refractive index is adjusted to be within 0.02% of that of the grains using a mix of oils [22]. In the case of a flat bed, this conical geometry results in circular fluid flow with a uniform shear rate $\dot{\gamma}$ across the bed surface given by $\dot{\gamma} = 2\pi f/\tan\beta$, where β is the angle between the conical surface and the bed surface [9]. The corresponding shear stress τ normalized by the non-buoyant weight of the grains is given by $\tau^* = \tau/(\rho_g - \rho_f)gd$, where, g is the acceleration due to gravity. By measuring τ using a torque sensor attached to the container as discussed in the Supplementary Documentation [23], we obtain τ^* and the corresponding value τ_c^* when steady state bedload transport occurs.

We image a vertical plane inside the bed at a distance

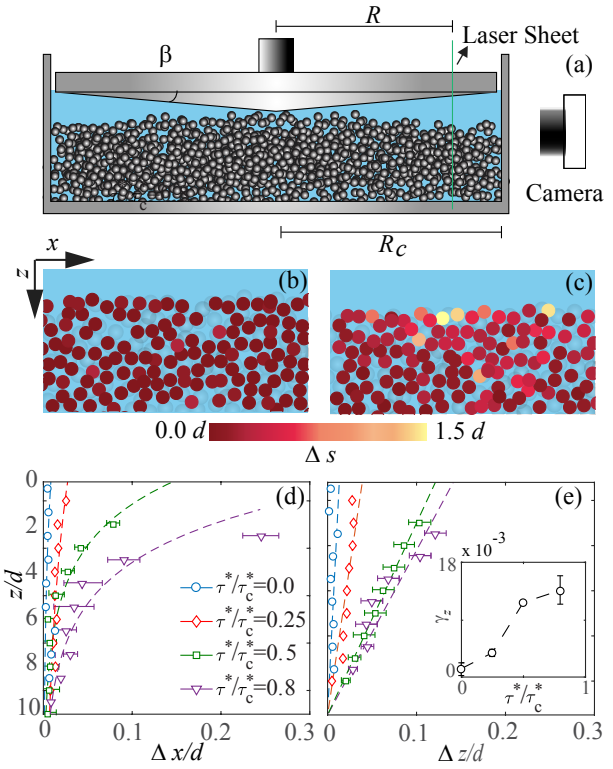

FIG. 1. (a) A schematic of the experimental apparatus which consists of a cylindrical container filled with transparent grains and fluid. The top plate is rotated about its axis to apply shear. (b,c) The final measured positions of the grains after $t = 5400\,\mathrm{s}$ corresponding to $\tau^*/\tau_c^* = 0.0$ (b), and $\tau^*/\tau_c^* = 0.8$ (c). The net displacement s of each grain is shown by the color bar. (d,e) The mean displacement of the grains over 60 seconds near the initial onset of shear, in the flow direction (d) and gravity (e) as a function of depth z from the bed surface. The dashed lines in the two graphs correspond to exponential and linear fits, respectively. (e) Inset: The strain gradient γ_z as a function of τ^*.

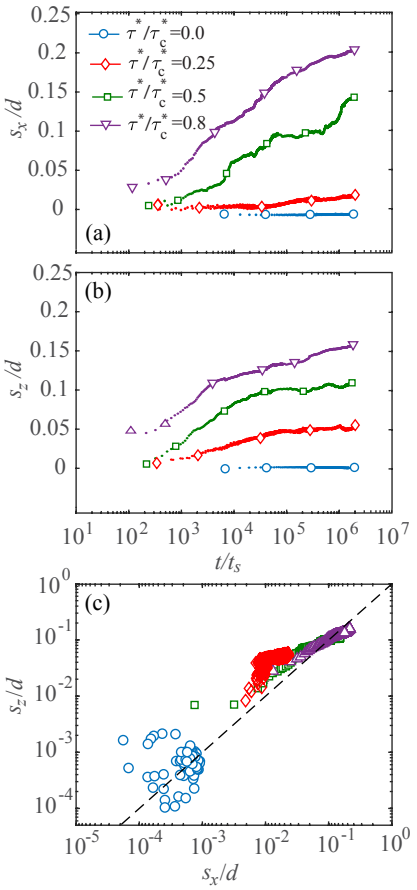

FIG. 2. The cumulative displacement of the top layer of the bed in the x (a) and z (b) direction over 48 hours are observed to increase quickly before settling out to a slow creep systematically larger with larger τ/τ^*. (c) s_x versus s_z fall near a line with slope one, showing that the rearrangements in the two directions are correlated above $\tau^*/\tau_c^* = 0.0$.

of $R = 72\,\mathrm{mm}$ from the central axis which is also $12d$ away from the side walls to avoid any direct influence of the boundaries. At this relatively large $R/d \approx 50$ and a sufficiently small viewing area, the region of interest can be modeled as planar, with flow moving from the left to the right. A Cartesian coordinate system is used to describe the system with the x-axis along the flow, the z-axis along gravity, and the y-axis pointing into the plane. We use a camera combined with a high pass filter to image the system illuminated with a vertical 532 nm laser sheet. The centroid of the dark pixels corresponding to each grain is used to determine its position within $0.02d$ in the $x - z$ plane [8]. Further, the diameter of the grain crosssection in the illumination plane is used to track grains within a distance $y \pm 0.22d$ from the center of the laser sheet.

Fig. 1(b) and Fig. 1(c) show examples of grain positions recorded after 90 minutes, corresponding to $\tau^*/\tau_c^* = 0.0$ and 0.8, respectively. Here, grains which remain within $y = \pm 0.16d$ are tracked and analyzed. The magnitude of displacement of the individual grains s in the plane over this time interval is denoted using the color map to capture the bed evolution. One observes that both beds rearrange, with greater motion occurring for $\tau^*/\tau_c^* = 0.8$. We obtain the average displacement in a short window of time, and plot the grain displacement in the direction of the flow and gravity in Fig. 1(d) and (e), respectively for various τ^*/τ_c^*. The time interval over which displacements are calculated corresponds to $t = 30\,\mathrm{s}$ and $t = 90\,\mathrm{s}$, and $z = 0$ is taken to be the surface of the freshly sedimented bed. One observes that the bed creeps forward faster and settles further with increasing τ^*. As shown by the fits, the creep along the flow direction appears to decay somewhat exponentially with depth. The decay length from the exponential fit in the case of the higher shear rates, where a meaningful

variation occurs, is found to be $2.5d \pm 0.1d$. This decay is similar to the length scale over which grain speeds exponentially decay into the bed for $\tau^* > \tau_c^*$ [8], and was observed to be common to dry granular beds in gravity which are sheared horizontally at the top [22, 24]. On the other hand, the linear compaction with depth at all shear rates implies that the bed settles uniformly as grains rearrange in gravity. The strain gradient $\gamma_z = -\Delta z/z$ obtained from the linear fit is shown in Fig. 1(e) and observed to be non-zero and increase significantly with τ^*.

To examine this relaxation of the bed over prolonged periods, we plot the average normalized displacement of the grains between $0 < z < 2d$ in the flow direction $s_x = \langle \Delta x \rangle$ and the gravitational direction $s_z = \langle \Delta z \rangle$ in Fig. 2(a) and (b), respectively, over 48 hours under steady $\dot{\gamma}$ conditions. Time t is normalized by the sedimentation time scale in our system t_s of a grain in the fluid due to gravity, i.e. $t_s = 18\nu/(\rho_p - \rho_f)gd = 0.11\,\mathrm{s}$, which is a typical time scale relevant to understanding grain-fluid systems. We observe that the grains continue to creep over the entire duration of the experiments over a million times t_s. Although, the overall rates are observed to decrease systematically over time, the bed creeps nonetheless over the entire time interval studied. The bed also initially settles rapidly, before slowing over time.

We plot s_x versus s_z in Fig. 2(c) to examine the correlation of the observed bed creep and consolidation. In the case of $\tau^* = 0$, we observe a scatter of points around the line with slope one indicating that the rearrangements are somewhat uncorrelated in the horizontal and vertical direction. Whereas, the amount of creep appears to be correlated with the amount of movement in the bed for $\tau^* > 0$, with greater creep corresponding to greater consolidation. While, the amount of creep is lower than the displacement along gravity at lower τ^*, the creep increases faster than the compaction due to gravity for $\tau^* \to \tau_c^*$.

We next study the evolution of the volume fraction of the grains ϕ to understand these trends in the bed relaxation. Fig. 3(a) shows an example of ϕ variation with depth, which is observed to increase sharply at the bed surface, reaching an essentially constant value within fluctuations for $z/d > 2$. The bed surface settles with increasing t as evident from the shift downward of ϕ in the $z - t$ plane in Fig. 3(a). This is consistent with the displacement of the bed surface over time seen in Fig. 2(b), where s_z was observed to increase with τ^*. We also examine the average granular volume fraction in the bed $\phi_g = \langle \phi \rangle$ in Fig. 3(c) to quantify the net effect of this relaxation as a function of time, where $\langle .. \rangle$ corresponds to averaging over the depth $z/d > 2$. We find that ϕ_g increases over time in each case, with faster increase for higher τ^*. Thus, a higher packing fraction is reached for higher τ^* over 48 hours. We also observe in the case of the higher τ^* that ϕ_g rises, and saturates around 0.64.

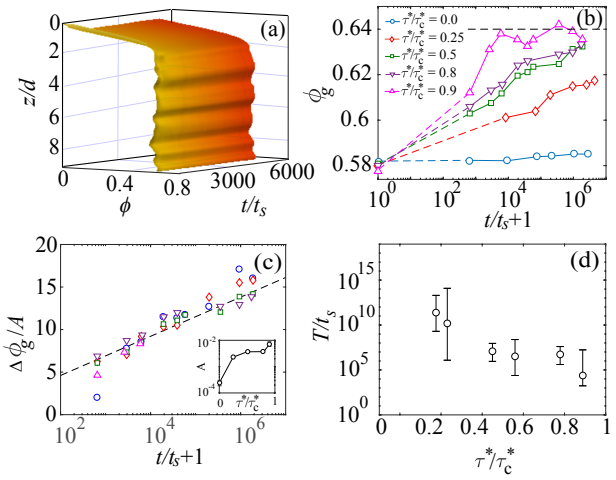

FIG. 3. (a) The volume fraction ϕ evolution as a function of depth for $\tau^*/\tau_c^* = 0.8$ averaged over 10 experiments. (b) Average granular volume fraction ϕ_g rises increasingly rapidly with τ^* before approaching ϕ_{rcp} indicated by dashed horizontal line. (c) The change in ϕ_g scaled with A in the regime where $t/t_s \gg 1$ and where $\phi_g < \phi_{rcp}$. The data is observed to collapse on the line corresponding to Eq. 1. Inset: The fitted A as a function of τ^*. (d) The time scale T over which ϕ_g increases to ϕ_{rcp} decreases rapidly as $\tau^* \to \tau_c^*$.

This volume fraction corresponds to the random close packing fraction $\phi_{rcp} = 0.64 \pm 0.02$ that spherical grains approach when the glass transition is reached [25, 26].

It has been also shown that the volume fraction of randomly created spherical grains are well below the maximum volume fraction for spheres $\phi_{max} = 0.74$ [27, 28], unless special protocols are used [29, 30]. When vibrated or tapped, such packings compact rapidly at first with compaction growing logarithmically over long times as they approach ϕ_{rcp} [19, 20, 31]. This logarithmic slowing dynamics has been explained using the parking lot model [32], where increasingly large number of grains have to rearrange collectively to create space which is sufficient to fit an additional grain and thus increase the total volume fraction.

To compare the compaction dynamics, we evaluate the change of volume fraction from the initial value before shear is applied

$$\Delta\phi_g = \phi_g - \phi_o = A \ln(1 + t), \qquad (1)$$

where, ϕ_o and A are constants related to initial conditions and system properties, and time has been shifted by one to avoid the singularity at $t = 0$. Fig. 3(c) shows $\Delta\phi_g$ obtained in our experiments scaled by A plotted versus time t corresponding to Eq. 1, with the fitting constant A shown in the inset. We observe a good collapse of the data over 4 orders of magnitude in the regime after the initial rapid transient regime and before ϕ_{rcp} is reached. Thus, we observe similar granular compaction dynam-

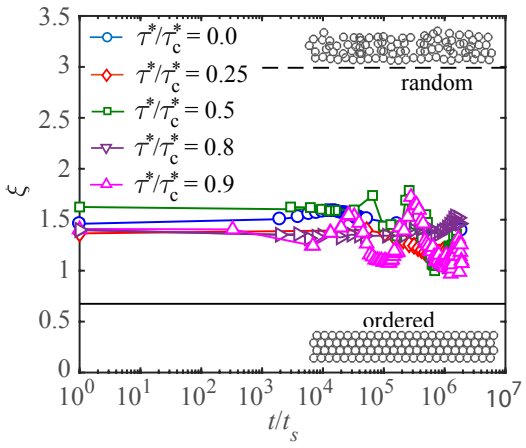

FIG. 4. Surface roughness ξ evolution for various τ^* shown in Fig. 3(b). The values corresponding to random and ordered hexagonal packings near the surface are also shown.

ics under sub-critical hydrodynamic shear as in vibrated systems [19, 20, 31–33]. Like the acceleration strength in the vibration experiments, the compaction logarithmically approaches ϕ_{rcp} faster as τ^* is increased. The major difference between these systems is the continuous versus discrete forcing as well as the steady creep in the horizontal direction under shear. Creep in turn also imparts energy to the bed as the grains fall and collide with the grains below, possibly causing momentum to percolate deep into the bed, similar to the taps in the vibrated experiments. As the bed approaches a jammed state it becomes increasingly unlikely for grains to rearrange without the participation of larger and larger numbers of grains. Hence, the compaction dynamics slows as ϕ_{rcp} is approached.

In Fig. 3(d) the time T that it takes the bed density to reach random close packing is shown assuming the logarithmic increase continues until the bed saturates at ϕ_{rcp}. One finds that the time that it takes for the bed to compact changes dramatically with τ^*. Although some compaction is observed at $\tau^* \approx 0$, the time scales obtained to reach ϕ_{rcp} are greater than the lifetime of the universe, and therefore not shown. At somewhat larger τ^*, we find that T decreases from about six centuries to the highest τ^*/τ_c^* studied, where T is of order of half an hour as τ_c^* is approached.

Finally, we examine the bed roughness to understand its contribution to the evolution of the creep. From Fig. 3(a), we note that the roughness of the bed surface can be characterized by using the rate at which ϕ increases at the bed surface. We obtain the roughness measure ξ by calculating the change of depth z where ϕ increases from 0.1 to 0.4, corresponding to roughly half the observed variation in ϕ. Plotting this measure ξ as a function of time in Fig. 4, we find that the roughness of the bed can vary somewhat but not systematically over the entire duration of the experiment in the case of each τ^*. For reference, we also calculated ξ corresponding to the case where the bed was ordered in a hexagonal lattice and a random surface. The random surface is created by randomly moving grains from a triangular lattice from a uniform distribution between 0 and d resulting in the grain positions shown in Fig. 4. We observe that the variation in ξ is relatively small compared to these two limits, and the bed surface roughness is essentially unchanged as ϕ_g varies from 0.58 to 0.64 over time for the various τ^*. The lack of significant change toward the ordered value shows that the presence of shear does not appear to make the bed surface any smoother by selectively eroding particles that protrude further into the fluid. Thus, we find that decrease in creep and consolidation show no significant correlation with the observed fluctuations in bed surface roughness.

In conclusion, we show with internal imaging that a freshly sedimented bed consolidates and creeps slowly over long times under sub-critical hydrodynamic shear conditions. While a small degree of consolidation is observed even when no shear is applied, the presence of shear stress causes rearrangements to increase and the grains to settle to a much greater degree. We find that the dynamics is similar to compaction in vibrated granular beds, and further illustrate how the rearrangements progress inside the bed, which has not been shown previously even in those studies. Thus, our results have broad implications for granular systems which may appear stationary at short time scales but in which significant grain movement and changes in bed strength occur over long time scales.

This work was supported by the National Science Foundation Grant CBET-1335928, and the US Department of Energy Office of Science, Office of Basic Energy Sciences program under DE-FG02-13ER16401.

[1] A. Shields, Mitteilungen der PreuBischen Versuchsanstalt fr Wasserbau **26** (1936).
[2] J. M. Buffington and D. R. Montgomery, Water Resource Research **33**, 1993 (1997).
[3] A. Recking, F. Liébault, C. Peteuil, and T. Jolimet, Earth Surface Processes and Landforms **37**, 774 (2012).
[4] F. Charru, H. Mouilleron, and O. Eiff, Journal of Fluid Mechanics **519**, 55 (2004).
[5] H. Mouilleron, F. Charru, and O. Eiff, Journal of Fluid Mechanics **628**, 229 (2009).
[6] J. Derksen and R. Larsen, Journal of Fluid Mechanics **673**, 548 (2011).
[7] M. Houssais, C. P. Ortiz, D. J. Durian, and D. J. Jerolmack, Nature Communications **6**, 6527 (2015).
[8] B. Allen and A. Kudrolli, Physical Review Fluids **2**, 024304 (2017).
[9] A. Kudrolli, D. Scheff, and B. Allen, Journal of Fluid Mechanics **808**, 397.

[10] J. Tsai, G. Voth, and J. Gollub, Physical Review Letter **91**, 064301 (2003).
[11] A. E. Lobkovsky, A. V. Orpe, R. Molloy, A. Kudrolli, and D. H. Rothman, Journal of Fluid Mechanics **605**, 47 (2008).
[12] M. Ouriemi, P. Aussillous, and É. Guazzelli, Journal of Fluid Mechanics **636**, 295 (2009).
[13] A. Hong, M. Tao, and A. Kudrolli, Physics of Fluids **27**, 013301 (2015).
[14] A. H. Clark, M. D. Shattuck, N. T. Ouellette, and C. S. O'Hern, Physical Review E **92**, 042202 (2015).
[15] S. W. Smith and M. Wyss, Bulletin of Seismological Society Am. **58**, 1955 (1968).
[16] R. Bucknam, G. Plafker, and R. Sharp, Geology **6**, 170 (1978).
[17] C. Marone, C. Scholz, and R. Bilham, Journal of Geophysical Research **96**, 8441 (1991).
[18] S. Nasuno, A. Kudrolli, and J. Gollub, Physical Review Letter **79**, 949 (1997).
[19] J. B. Knight, C. G. Fandrich, C. N. Lau, H. M. Jaeger, and S. R. Nagel, Physical Review E **51**, 3957 (1995).
[20] P. Ribiére, P. Phillipe, P. Richard, R. Delannay, and B. D., Journal of Physics: Condensed Matter **17**, S2743 (2005).
[21] J. Ren, J. Dijksman, and R. Behringer, Physical Review Letters **110**, 018302 (2013).
[22] S. Siavoshi, A. V. Orpe, and A. Kudrolli, Physical Review E **73**, 010301 (2006).
[23] The measurement of the shear stress as a function of applied strain rate can be found in the supplementary documentation.
[24] D. Henann and K. Kamrin, Proceedings of the National Academy of Sciences **110**, 6730 (2013).
[25] J. G. Berryman, Phys. Rev. A **27**, 1053 (1983).
[26] C. S. O'Hern, S. A. Langer, A. J. Liu, and S. R. Nagel, Phys. Rev. Lett. **88**, 075507 (2002).
[27] G. D. Scott and D. M. Kilgour, Journal of Physics D **12**, 863 (1969).
[28] G. Onoda and E. Liniger, Physical Review Letters **64**, 2727 (1990).
[29] A. Panaitescu, K. Anki Reddy, and A. Kudrolli, Physical Review Letters **108**, 108001 (2012).
[30] A. Panatescu and A. Kudrolli, Physical Review E **90**, 032203 (2014).
[31] P. Philippe and D. Bideau, Europhysics Letters **60**, 677 (2002).
[32] E. Ben-Naim, J. Knight, E. Nowak, H. M. Jaeger, and S. Nagel, Physica D **123**, 380 (1998).
[33] P. Richard, M. Nicodemi, R. Delannay, P. Ribiére, and D. Bideau, Nature Materials **4**, 121 (2005).